Universitat Politècnica de Catalunya
Escola Superior d'Enginyeria de Telecomunicació de Barcelona
Grau en Enginyeria Física

Thermal radiation measurements of Silicon microspheres

Salim Benadouda i Ivars

Directors: Ramon Alcubilla i Moisés Garín

Barcelona, Juny 2017

Abstract

Mie's solution to Maxwell's equations describes the interaction of a light wave with a sphere. This solution - for sphere dimensions comparable to the light wavelength- has a very a interesting result. For some resonant frequencies and sphere radii, scattering section can be more than ten times greater than actual geometric section. Furthermore, under some conditions, the absorption cross section can also be larger than the real one. This means that the microsphere would absorb more light than the one impinging on its surface. This would have a very impressive consequence on light harvesting. In order to test this ability and applying Kirchhoff's law of thermal radiation - which states that the emissivity is equal to the absorptivity - we would measure thermal radiation of a single microshpere.

In this project we design a optical set-up that will be part of the final set-up used to measure the thermal radiation of a single microsphere. In order to perform the measurement Step-Scan FT-IR spectroscopy combined with lock-in techniques were used. We where able to measure an area of $10\mu m$ radius' circle in contrast to the few millimetres that normal FT-IR measures.

Acknowledgements

I would like to express my gratitude to everyone that has helped me to realise this project, either with knowledge or moral support. First of all my supervisor Moisés for his guidance and his advice. Thank you so much. Also Ramon Alcubilla for being there always when everything was going wrong. To Xavi and Miguel for being so nice and comprehensive. To Laura for welcome me to her lab when mine was not accessible. To Vicenta for everything. And to all my friends and family who have provided much necessary support in stressful moments.

Special thanks to José and Jaume from la FIB for being there always, always. *Que no tot en la vida és faena.*

Contents

List of Tables

List of Figures

Chapter 1

Introduction

When speaking of semiconductors we must speak of Silicon. The importance of Silicon has its reasons. Its natural abundance, a convenient band gap or an easy forming oxide (SiO_2) used as an insulator and passivisation layer. Thus, Silicon has become a very well known material that has built a whole technology around it. Nowadays, it is possible to grow huge pure monocrystalline blocks as well as micro- and nano- scale structures.

Silicon colloids 1.1, that are extremely spherical particles, have been capturing the attention of researchers lately. These colloids have sizes varying from nanometers to micrometers, comparable to light wavelength on the Infrared region.

Additionally, Silicon's high refractive index and highly sphere-like shape drive the colloids to behave like good resonators according to Mie's theory. [6][7]

There are many potential applications for Silicon microspheres, especially concerning their ultrahigh quality factor resonances. A very interesting application is the production of solar cells with these microspheres. When they trap photons in Mie resonances, these photons stay long periods of time in there, which is equivalent to travel hundreds of micrometers in bulk silicon. Thanks to that, higher efficiency can be achieved with less Silicon. [2].

Another interesting application is using these colloids as solar filter. A sunscreen based on a mixture of oil and water with the microspheres was compared with a commonly used sunscreen

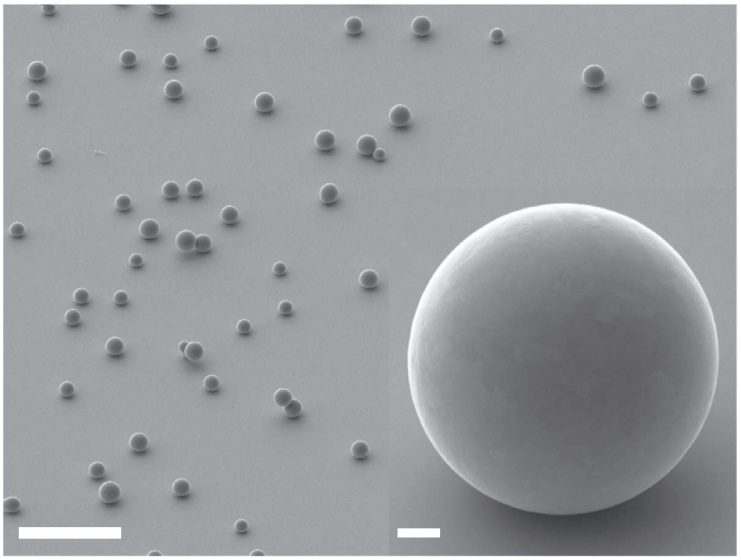

Figure 1.1: SEM images of spherical Silicon polydisperse colloids from [2]

with TiO_2 nanoparticles - with the same concentration in weight of particles in both cases -[8]. Silicon particle based sunscreen performed better than the TiO_2 one in UV, VIS and IR regions.

Initially, the aim of this project was the development of an experimental set-up to thermally characterise these microspheres. However, due to several inconveniences encountered during the process, only the optical set-up was carried out (and not the thermal set-up). The addition of the thermal set-up, once the optical one has been achieved, would be straightforward though not trivial. More details on both set-ups will be discussed in section 2.3. It must be noted that throughout the whole document thermal characterisation will be referred to as the main goal of all the involved processes.

1.1 Thermal Radiation

Light harvesting in solar cells relies on absorption of light of the semiconductor. The absorption coefficient is the fraction of incident light that is absorbed by the body when radiating and absorbing in thermodynamic equilibrium. Similarly, the power emitted by an arbitrary body of a fixed size and shape at an explicit temperature can be described by a dimensionless coefficient,

emissivity. This number is the ratio of emissive power of the body to the power that a perfect Black Body of same size, shape and temperature would emit.

Assuming these definitions, Kirchhoff's law of thermal radiation states that for an arbitrary body emitting and absorbing thermal radiation in thermodynamic equilibrium, the emissivity is equal to the absorptivity. We can also extract from the law that emissivity cannot exceed one, which means that it is impossible to thermal radiate more energy than an ideal Black Body. So an ideal Black Body would have $\epsilon_{\mathrm{BB}} = 1$ while every other body $\epsilon(\lambda) < 1$. The thermal power of the emitter follows Stefan-Boltzman law:

$$P = \sigma_{\mathrm{sb}} \epsilon A T^4 \tag{1.1}$$

where T is the surface temperature, A the surface area, ϵ the emissivity of the body and σ_{sb} the Stefan-Boltzmann constant.

Nowadays, these limits have been challenged at the nano- and micro- scale, where sizes of the emitters (absorbers) are comparable to light wavelength.

1.1.1 Black Body Radiation

A Black Body is an idealised physical body that can absorb all incident electromagnetic radiation independently of the frequency or angle of incidence. Hence, a Black Body does not reflect or transmit radiation making it a perfect emitter as it has to emit all the energy that it absorbs.

Plank's law (1.2) describes the spectral radiance of electromagnetic radiation emitted by a Black Body at a given temperature. It describes the amount of energy as radiation at different frequencies, and it is measured in terms of the power emitted per unit area, unit solid angle and per unit frequency.

$$L_{\mathrm{BB}}(\lambda, T) = \frac{2hc^2}{\lambda^5} \frac{1}{e^{\frac{hc}{\lambda k T}} - 1} \tag{1.2}$$

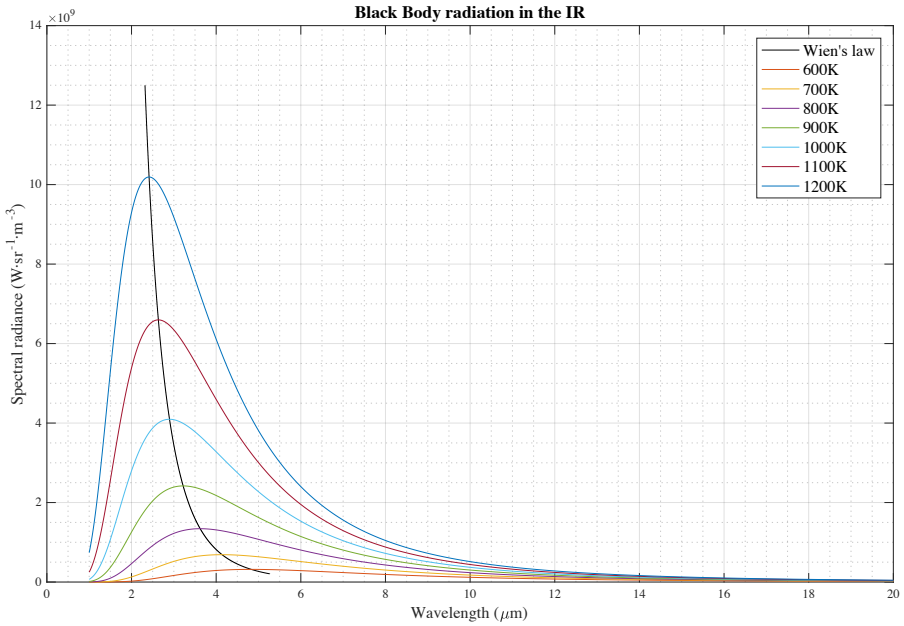

Figure 1.2: Theoretical Black Body radiation a different temperatures and Wien's law

We can extract two basic features:

- Total emitted power at all wavelength increases with temperature *i.e.* the curve's integral increases with temperature)
- The wavelength for the maximum emittance shifts to lower wavelength with increasing temperature. Wien's law (equation 1.3) states that the curve for different temperatures peaks at a wavelength of the Black Body radiation is inversely proportional to the temperature as we can see in Figure 1.2.

$$\lambda_{max} = \frac{b}{T} \tag{1.3}$$

As already stated, for a given temperature, we can define the emittance as:

$$\epsilon\left(\theta, \varphi, \lambda, T\right) = \frac{B\left(\theta, \varphi, \lambda, T\right)}{B_{BB}\theta, \varphi, \lambda, T} \leq 1 \tag{1.4}$$

At the same temperature, all other emitters will produce a lower power than a Black Body [9].

However, introducing Mie's solution to Maxwell's equations, some structures can achieve higher power with respect to their size than a Black Body. It is to note, that this property is local,

when analysing the macroscopical radiation Kirchhoff's law is still respected. Microshperes are supposed to show this behaviour. [7]

1.2 Light Scattering

Light scattering is present in our daily life. The colour of the sky can be explained using Rayleigh scattering theory; or rainbows, that are light scattered by cloud particles surrounded by water vapour in the atmosphere. The scattering theory for a spherical particle was developed by Mie in 1908. This theory describes the scattering response to an electromagnetic radiation of the particle when its size is of the order of the incident wavelength.

When light collides with a random particle (Figure 1.3), light will be scattered in all directions of space. There is also a part of the electromagnetic radiation that will be absorbed by the particle, so the resulting wave will be attenuated with respect to the original one. From now on, we will

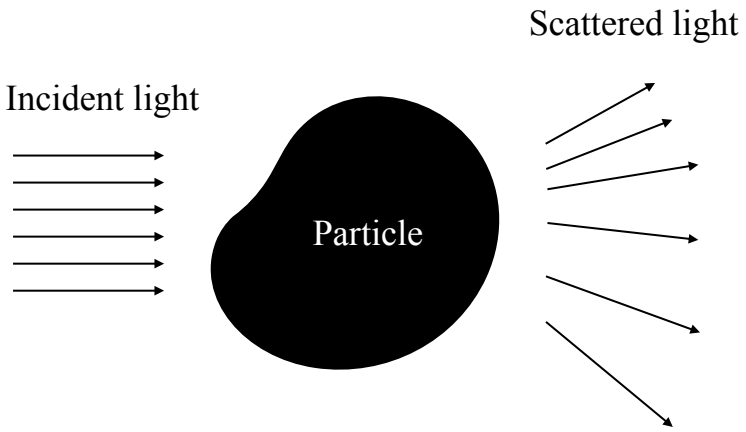

Figure 1.3: Scattering of light by a random particle. The particle will absorb and scatter the radiation in all directions

assume elastic scattering, that is to say that the scattered wave will have the same frequency that the incident one. Moreover, our radiation source is not powerful enough to provoke non-linear phenomena [6]. In the following section we will introduce the scattering theory in Mie regime. We will study microspheres with sizes of the same order of the electromagnetic radiation (we are interested in wavelength from $\sim 2\mu m - 12\mu m$).

1.2.1 Mie Resonance

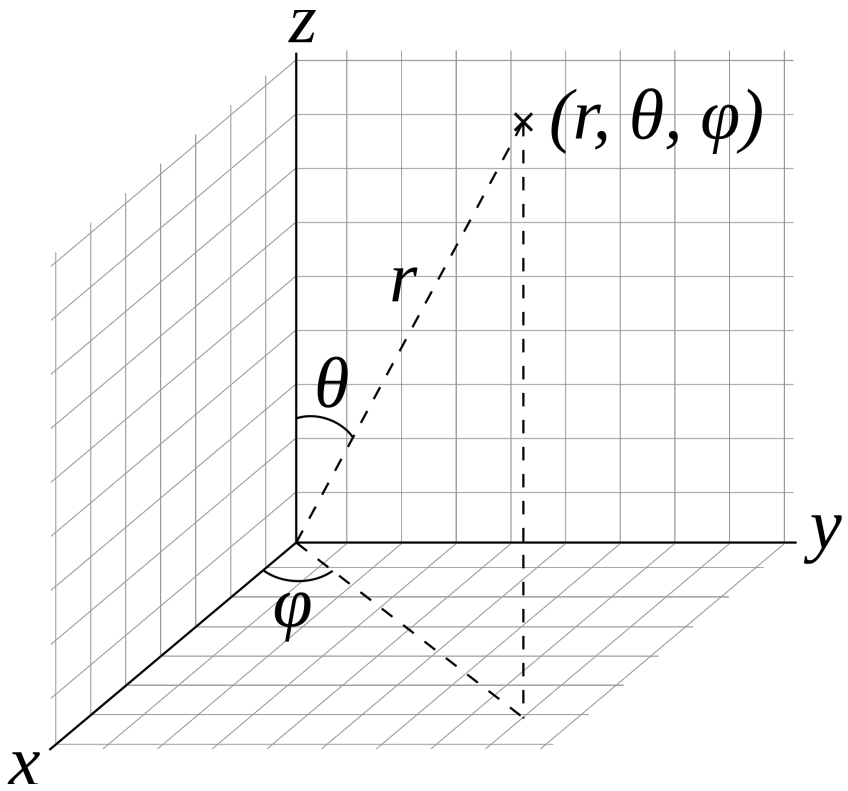

Figure 1.4: Spherical coordinates (r, θ, φ). Where r is the radial distance, θ the polar angle and φ the azimuthal angle.

Mie's solution to Maxwell's equations describes the scattering of a wave by a sphere. The formal solution for the sphere in a medium based on Mie theory can be expressed in the form of equations that explicitly exhibit the refractive index of the medium as well as that of the sphere. The equations are formally identical for an absorbing medium where both refractive indexes can have an imaginary component. In order to solve the equations, a spherical coordinate system (Figure 1.4) has to be used.

We consider the scattering of a wave by a sphere with radius r_0 embedded in an absorbing medium with a refractive index n. The origin of the coordinate system is placed in the centre of the sphere and the positive z axis is placed along the direction of propagation of the incident wave. This way, the scattered electric $\mathbf{E_s}$ and magnetic $\mathbf{H_s}$ fields can be expressed like [10][11]:

$$\mathbf{E_s} = \sum_{n=1}^{\infty} E_n \left(i a_n \mathbf{N}_{e1n}^{(3)} - b_n \mathbf{M}_{o1n}^{(3)} \right) \tag{1.5}$$

$$\mathbf{H_s} = \frac{k}{\omega\mu}\sum_{n=1}^{\infty} E_n \left(a_n \mathbf{M}_{e1n}^{(3)} + i b_n \mathbf{N}_{o1n}^{(3)}\right) \tag{1.6}$$

with

$$E_n = i^n E_0 \frac{2n+1}{n\,(n+1)} \tag{1.7}$$

Where k is the propagation constant, ω the angular frequency and μ the permeability of the medium, E_0 the amplitude of the incident electric field and i is the imaginary unit. The superscript $^{(3)}$ indicates the type of Bessel function $z_n(\rho)$, in this case it is $h_n^{(1)}$. The spherical Bessel function of the third kind is defined as follow:

$$h_n^{(1)}(\rho) = j_n(\rho) + i y_n(\rho) \tag{1.8}$$

where j_n and y_n are the spherical Bessel function.

$$j_n(\rho) = (-\rho)^n \left(\frac{1}{\rho}\frac{\mathrm{d}}{\mathrm{d}\rho}\right)^n \frac{\sin\rho}{\rho} \tag{1.9}$$

$$y_n(\rho) = -(-\rho)^n \left(\frac{1}{\rho}\frac{\mathrm{d}}{\mathrm{d}\rho}\right)^n \frac{\cos\rho}{\rho} \tag{1.10}$$

and $\mathbf{M}_{01n}$, $\mathbf{M}_{e1n}$, $\mathbf{N}_{01n}$ and $\mathbf{N}_{e1n}$ are given by (note that $\mathbf{e}_r, \mathbf{e}_\theta$ and $\mathbf{e}_\varphi$ stand for the unit vectors of the spherical coordinate system):

$$\mathbf{M}_{o1n} = \cos\varphi\,\pi_n(\cos\theta)\,h_n^{(1)}\mathbf{e}_\theta - \sin\varphi\,\tau_n(\cos\theta)\,h_n^{(1)}\mathbf{e}_\varphi \tag{1.11}$$

$$\mathbf{M}_{e1n} = -\sin\varphi\,\pi_n(\cos\theta)\,h_n^{(1)}\mathbf{e}_\theta - \cos\varphi\,\tau_n(\cos\theta)\,h_n^{(1)}\mathbf{e}_\varphi \tag{1.12}$$

$$\begin{aligned}\mathbf{N}_{o1n} &= \sin\varphi\,n\,(n+1)\sin\theta\,\pi_n(\cos\theta)\,\frac{h_n^{(1)}}{\rho}\mathbf{e}_r \\ &+ \sin\varphi\,\tau_n(\cos\theta)\,\frac{\left[\rho h_n^{(1)}\right]'}{\rho}\mathbf{e}_\theta + \cos\varphi\,\pi_n(\cos\theta)\,\frac{\left[\rho h_n^{(1)}\right]'}{\rho}\mathbf{e}_\varphi\end{aligned} \tag{1.13}$$

$$\begin{aligned}\mathbf{N}_{e1n} &= \cos\varphi\,n\,(n+1)\sin\theta\,\pi_n(\cos\theta)\,\frac{h_n^{(1)}}{\rho}\mathbf{e}_r \\ &+ \cos\varphi\,\tau_n(\cos\theta)\,\frac{\left[\rho h_n^{(1)}\right]'}{\rho}\mathbf{e}_\theta - \sin\varphi\,\pi_n(\cos\theta)\,\frac{\left[\rho h_n^{(1)}\right]'}{\rho}\mathbf{e}_\varphi\end{aligned} \tag{1.14}$$

where π_n τ_n are defined as:

$$\begin{aligned} \pi_n &= \frac{P_n^1}{\sin\theta} \\ \tau_n &= \frac{dP_n^1}{d\theta} \end{aligned} \tag{1.15}$$

With P_n^1 is the Legendre function of the first kind and $\rho = kr$ is being a dimensionless variable. Now, applying boundary conditions at the particle-medium interface we can find the coefficients a_n and b_n.

$$a_n = \frac{\mu m^2 j_n(m\alpha)\left[\alpha j_n(\alpha)\right]' - \mu_1 j_n(\alpha)\left[m\alpha j_n(m\alpha)\right]'}{\mu m^2 j_n(m\alpha)\left[\alpha h_n^{(1)}(\alpha)\right]' - \mu_1 h_n^{(1)}(\alpha)\left[m\alpha j_n(m\alpha)\right]'} \tag{1.16}$$

$$b_n = \frac{\mu_1 j_n(m\alpha)\left[\alpha j_n(\alpha)\right]' - \mu j_n(\alpha)\left[m\alpha j_n(m\alpha)\right]'}{\mu_1 j_n(m\alpha)\left[\alpha h_n^{(1)}(\alpha)\right]' - \mu h_n^{(1)}(\alpha)\left[m\alpha j_n(m\alpha)\right]'} \tag{1.17}$$

where a relative refractive index was m was introduced.

$$m = \frac{n_1}{n} \tag{1.18}$$

being $\tilde{n}_1$ and $\tilde{n}$ the refractive indices of the particle and the surrounding medium. These indices are complex and can be expressed as $\tilde{n} = n + i\kappa$ The permeability of the sphere, μ_1, appears in the expression. And we have introduced a new constant, the size parameter α.

$$\alpha = kr_0 = \frac{2\pi r_0}{\lambda} \tag{1.19}$$

From equations 1.5 and 1.6 we can see that $\mathbf{M}_n$ and $\mathbf{N}_n$ are EM normal modes of the spherical particle being the resulting EM scattered field the superposition of these modes weighted by coefficients a_n and b_n. We can see that TE modes are weighted by b_n and TM modes by a_n.

Now, we will take a closer look at the weights. Both coefficients depend on wavelength and as Bessel functions are oscillating we will expect very small denominators for some wavelengths. When this happens, the resulting electromagnetic field is dominated by the mode that "has achieved" the small denominator, thus, there will exist a resonance that is commonly noted as TM_{nm} or TE_{nm} being n the index of b_n or a_n that is much more greater than the others and m indexes the size parameter that achieves the resonance being 1 the lowest, 2 the next one and

so on.

Total light scattered and absorbed by the microsphere can be determined by the absorption cross section σ_a and the scattering cross section σ_s. We can obtain the scattering cross section by means of the energy conservation rules. It expression is the following:

$$\sigma_s = \frac{2\pi}{k^2} \sum_{n=1}^{\infty} (2n+1) \left(|a_n|^2 + |b_n|^2 \right) \tag{1.20}$$

In order to calculate the scattering cross section, we can use some available programs [6]. Some of them calculate the scattering efficiency Q_s that can be related to σ_s as follow:

$$Q_s = \frac{\sigma_s}{\pi r_0^2} \tag{1.21}$$

So this scattering efficiency checks the ratio of the optical scattering area with the actual geometric area seen by the radiation. Another interesting relation is the one concerning the extinction cross section. According to the definition of extinction:

$$\sigma_e = \sigma_a + \sigma_s \tag{1.22}$$

As done with scattering, we can define the extinction and absorption efficiency as

$$\begin{aligned} Q_e &= \frac{\sigma_e}{\pi r_0^2} \\ Q_a &= \frac{\sigma_a}{\pi r_0^2} \end{aligned} \tag{1.23}$$

and we can find that the expression of the extinction cross section is

$$\sigma_e = \frac{2\pi}{k^2} \sum_{n=1}^{\infty} (2n+1) \, \Re \left(a_n + b_n \right) \tag{1.24}$$

From equation 1.22 we get the final expression for absorption cross section

$$\sigma_a = \frac{2\pi}{k^2} \left[\sum_{n=1}^{\infty} (2n+1) \, \Re \left(a_n + b_n \right) - \sum_{n=1}^{\infty} (2n+1) \left(|a_n|^2 + |b_n|^2 \right) \right] \tag{1.25}$$

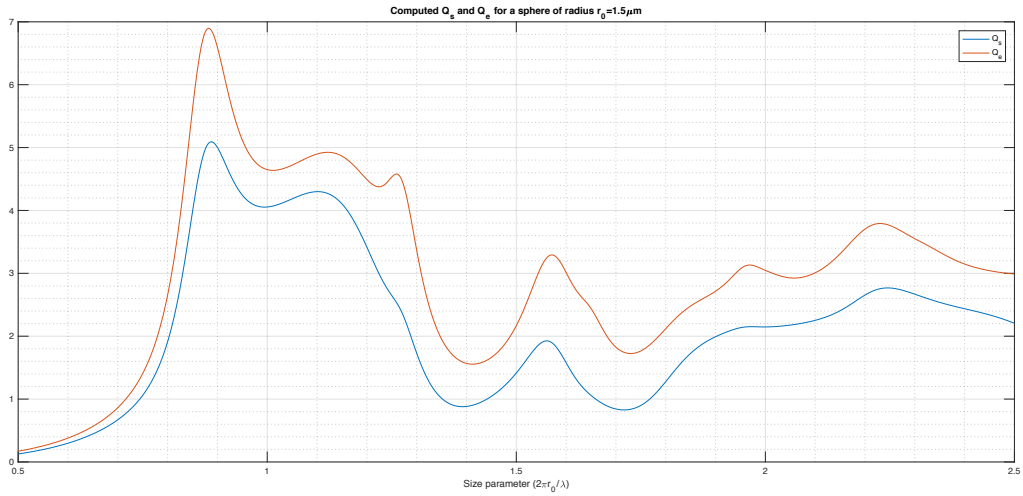

Figure 1.5: Scattering and extinction efficiency of a silicon sphere of $1.5\mu m$. A refractive index of $3.42 + i0.085$ has been used. First peak correspond to $TE_{1,1}$ and the second one to $TM_{1,1}$.

Using the code already mentioned, we can obtain Q_s, Q_e and Q_a. We can see in Figure 1.5 that the optical scattering and extinction are considerably larger than the geometric one. We also observe the peaks of the different resonances. It has to be noticed that the resonance has a high dependence on the refractive index of the particle.

For some resonant frequencies and radius, the scattering section can be more than ten times the actual geometric section. Moreover, under some conditions, the spheres can show an absorption cross section larger than the real section as shown in Figure 1.7. That would mean that the microspheres would be able to absorb more light than the actual light impinging them.

From now on we are going to focus on a single term of the sumations in equations 1.20, 1.24 and 1.25. We will refer them as σ'_s, σ'_e and σ'_a. Due to the strong dependence of the scattering and absorbing cross sections on $\tilde{n}$, high refractive particles as silicon have a very different spectra from lower index ones. We know that the strongest resonances in the case of Silicon correspond to low order resonances. We consider Mie resonances as classical resonators with Lorentzian line-shapes in order to simplify coming analysis.

If we want to get the maximum profit of the absorption of the sphere, we should find the values n and κ that maximise it. In fact, we will keep n fixed at 3.42 as we want to study this

absorption in the IR where silicon has a constant real refractive index. From [7] we know that

$$\sigma'_a\left(k = k_{max}\right) = \sigma'_s\left(k = k_{max}\right) = \frac{\sigma'_s\left(k = 0\right)}{4} \tag{1.26}$$

Using this relation, we can find the κ for which σ_a and consequently Q_a are maximum. The value for a sphere of $1.5\mu\, m$ is approximately $\kappa = 0.085$. This maximum is placed at a wavelength $\lambda = 7.4272\mu\, m$.

From 1.6 and using the relation that relates the absorption coefficient and the extinction coefficient:

$$\alpha_{abs} = \frac{4\pi\kappa}{\lambda} \tag{1.27}$$

We can find that this value of the extinction coefficient κ can be achieved by doping the silicon with the doping density N_D being between $3.210^{-}17cm^{-3}$ and $1.710^{-}17cm^{-3}$, that are achievable doping densities.

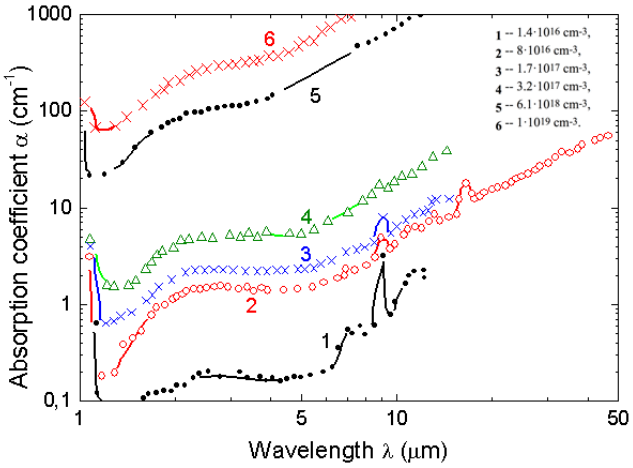

Figure 1.6: Free carrier absorption vs. wavelength at different doping levels. From [3]

As we speak of silicon - widely used in light harvesting - this effect has a very impressive consequence. As we said, according to Kirchhoffs law, emissivity would be higher than one. This would mean that when the microspheres would be heated, they would emit, with respect to their size, more than a Black Body. We have to take into account that even if a single sphere

is able to emit more than a Black Body, a macroscopical surface coated with microspheres would still exhibit an emission lower than one. Fulfilling thermodynamics laws.

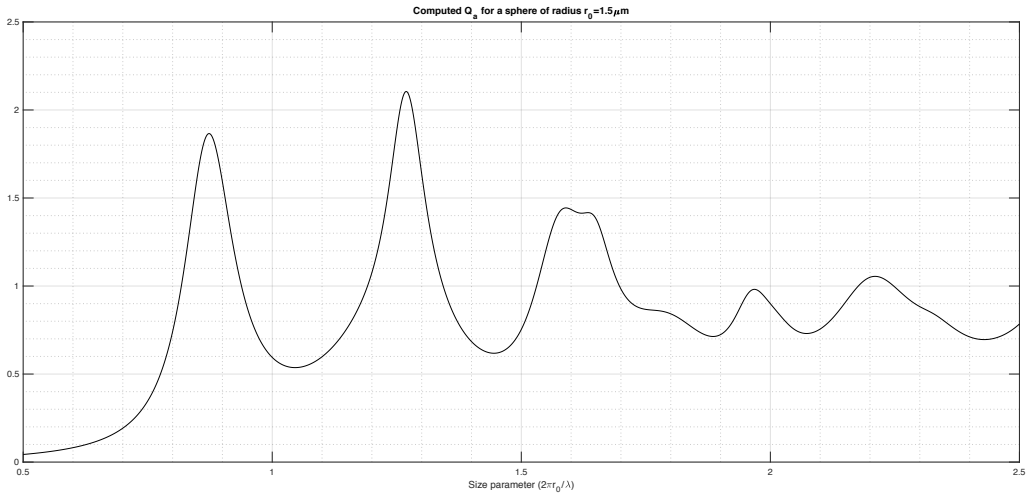

Figure 1.7: Absorption efficiency of a silicon sphere of $1.5\mu m$. A refractive index of $3.42+i0.085$ has been used. First peak correspond to $TE_{1,1}$ and the second one to $TM_{1,1}$

Chapter 2

Characterisation Techniques

Thermal characterisation of a single microsphere is not trivial. Ideally, we should isolate it in vacuum, heat it to a known and controlled temperature and then measure its emission. We are not able to perform that experiment; instead we want to measure the emissivity of a single sphere in a substrate and then try to separate the substrate emission from the desired emission. In order to do that, a Fourier Transform InfraRed spectrometer (FT-IR) will be used. All the set-up is placed outside the FT-IR and so, background radiation will be strongly taken into account. As the signal will be very low with respect to the ambient radiation, Lock-In techniques will be combined with the spectrometer. In this chapter we will briefly comment on the most relevant aspects of these techniques and the experimental set-up.

2.1 FT-IR Spectroscopy

2.1.1 The Michelson Interferometer

In order to understand FT-IR Spectroscopy, we should take a look at the Michelson Interferometer (Figure 2.1). First, let us consider a beam that comes from the source (S). The emitted beam is directed towards a beam splitter that divides light into to two equal beams, but one gets transmitted and the other reflected; so they follow different paths. The reflected wave

travels to the fixed mirror (M_1) and reflects back to the beam splitter. Let us assume that L is the length of the fixed arm of the interferometer. This way, the beam total path length will be $2L$. The same happens to the transmitted part of the beam. However, the second mirror (M_2) is not fixed. It can move a distance x, back and forward, from the zero displacement position L. Hence, the total path length for this wave will be $2L + x$. When both beams recombine at the beam splitter they exhibit an optical retardation $\delta = 2x$. After this, the beam leaving the interferometer is focused on the detector (D).

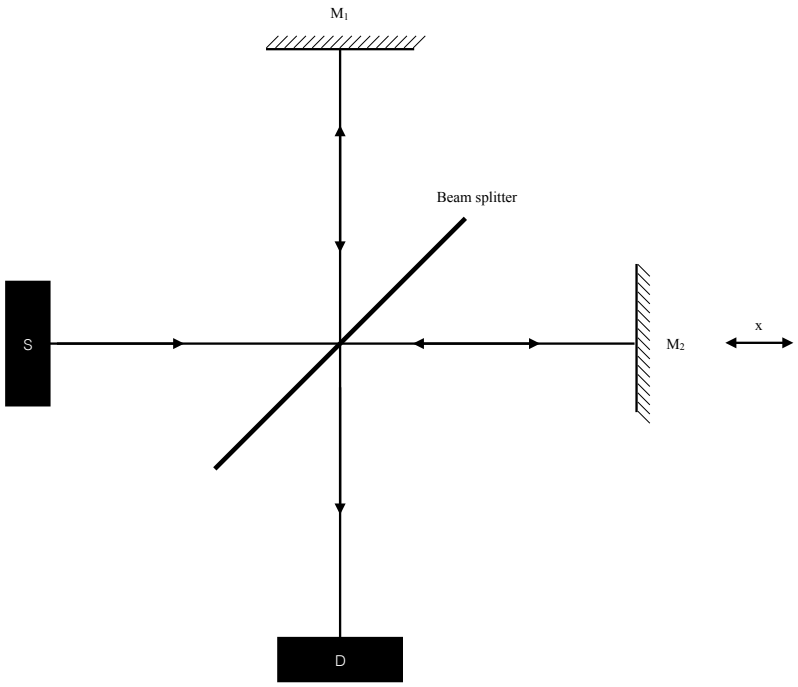

Figure 2.1: The Michelson Interferometer

The detector will measure the intensity $I(x)$ as a function of the mirror displacement. An example of an interferogram is shown in Figure 2.2. It has to be noted that the interferogram presented is single sided, meaning that data was not acquired for all possible negative displacement x. We will explain below why we can do this. Wave will recombine with different phases. Recombination would be constructive, yielding to a maximum detector signal when δ is an exact multiple of the wavelength of the beam.

$$\begin{aligned} \delta &= 2x = n\lambda \\ n &= 0, 1, 2... \end{aligned} \tag{2.1}$$

A destructive interference will take place when δ is an odd multiple of $\lambda/2$. We can write dependence of the intensity at the detector as:

$$I(x) = S(\nu) \cos 2\pi\nu x \tag{2.2}$$

We have defined wavenumber as $\nu = 1/\lambda$ and we have introduced $S(\nu)$ as the intensity of the monochromatic line at wavenumber ν. Sample spacing Δx is inversely proportional to $\Delta\nu$ so maximum resolution in wavenumbers will be determined by the step x of the machine. Time needed to move the mirror M_2 is very low, as the mirror moves very fast, so we can get full interferogram in fractions of a second [12]

In our case, this will not be like that since we will have to use a special mode of the FT-IR spectrometer called Step Scan [13][14]. Step Scan mode is a technique that has to be distinguished from the conventional Rapid Scan mode. In Rapid Scan mode the moving mirror of the Michelson interferometer moves continuously. This allows scanning a full spectrum in fractions of second, making possible the averaging of plenty of spectra. As opposed, Step Scan the mirror is moved a single step to a fixed position and held there making the path difference constant during a desired time. In the FT-IR that has been used, the computer connected to it can control the total number of detector digitisation for the averaging, the position of the mirror and the time that the mirror is retained at the fixed position. It has to be noted that FT-IR spectrometers - for Rapid Scan and Step Scan modes -, as opposed to conventional IR spectrometers, can record all frequencies of the IR beam at the same time.

2.1.2 Fourier Transform

In order to understand data harvested by the FT-IR, we must make a rough introduction to Fourier transform. Fourier transform decomposes a function of time into the frequencies that

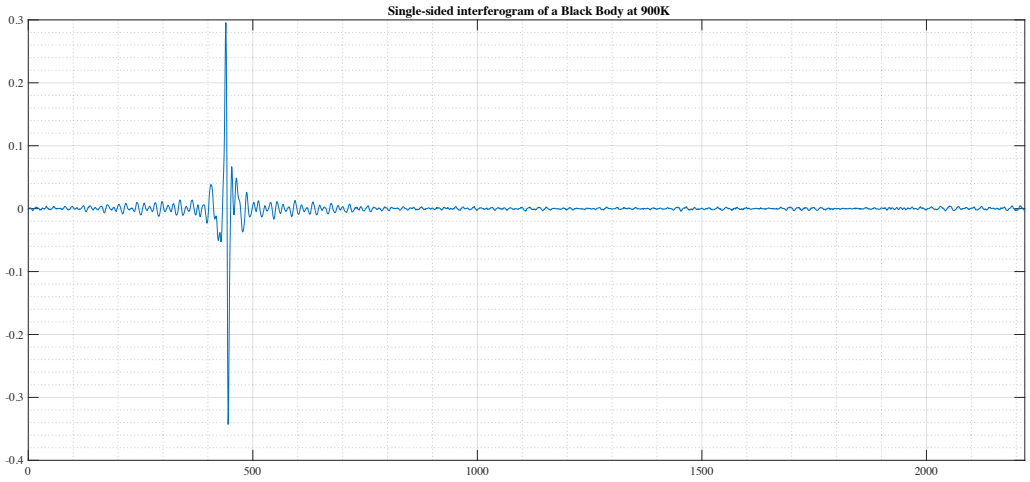

Figure 2.2: Signal measured by the detector. X axis is arbitrary. Y axis is the adimensional responce of the detector

build it up. The FT and the inverse FT are defined as follow:

$$\begin{aligned} F(\omega) &= \int_{-\infty}^{\infty} f(t)\, e^{-i\omega t} dt \\ f(t) &= \frac{1}{2\pi} \int_{-\infty}^{\infty} F(\omega)\, e^{i\omega t} d\omega \end{aligned} \tag{2.3}$$

$F(\omega)$ is called Fourier transform of $f(t)$ and is represented as $F(\omega) = \mathcal{F}[f(t)]$ and $f(t)$ is called the inverse Fourier transform of $F(\omega)$ and is represented as $f(\omega) = \mathcal{F}^{-1}[F(\omega)]$. Normally, $F(\omega)$ is said to be the frequency spectrum of f. Fourier Transform has been exhaustively studied, and can find properties of the transformation in plenty of books as in [15] . One interesting property that we will use in coming sections is the following:

$$\begin{aligned} X(\omega) &= \mathcal{F}[x(t)] \\ Y(\omega) &= \mathcal{F}[y(t)] \\ \mathcal{F}[x(t)\, y(t)] &= X(\omega) * Y(\omega) \end{aligned} \tag{2.4}$$

As we will be dealing with digitised signals, we introduce the discrete version of the transform, the Discrete Fourier transform (DFT), with the equivalent property ($\mathbf{x}_n$ is a sequence of N

complex numbers and $\mathbf{X}_n$ is the transformed sequence):

$$\begin{aligned}
\mathbf{X}_k &= \sum_{n=0}^{N-1} \mathbf{x}_n e^{-\frac{i2\pi kn}{N}} \\
\mathbf{x}_n &= \frac{1}{N} \sum_{k=0}^{N-1} \mathbf{X}_k e^{\frac{i2\pi kn}{N}} \\
\mathbf{Y} &= \mathcal{F}\left[\mathbf{y}\right] \\
\mathbf{X} &= \mathcal{F}\left[\mathbf{x}\right] \\
\mathcal{F}_k\left[\mathbf{xy}\right] &= \frac{1}{N}\left(\mathbf{X} * \mathbf{Y_N}\right)_k
\end{aligned} \tag{2.5}$$

2.1.3 Data Treatment

With the digitised interferogram $I(x)$ we must use the DFT in order to extract the spectrum $S(\nu)$. That is because our interferogram is a discreet series of N points. We will also replace continuous variables x and ν by $n\Delta x$ and $k\Delta\nu$ respectively. So applying equation 2.5 the discrete spectrum is expressed as follow.

$$S(k\Delta\nu) = \sum_{n=0}^{N-1} I(n\Delta x)\, e^{\frac{i2\pi nk}{N}} \tag{2.6}$$

Both spacing $\Delta\nu$ and Δx are related by

$$\Delta\nu = \frac{1}{N\Delta x} \tag{2.7}$$

The calculation of the spectrum must be done by computer. Plenty of DFT routines can be found on the internet and several books. But some numerical problems must be overcome [12][4]

First of all, if we recall equation 2.6, we see that the spectrum sampled at wavenumbers $k\Delta\nu$ can be computed from the interferogram at $\delta = n\Delta x$. Since n and k run from 0 to $N-1$, we will obtain a spectrum of N complex points. We would expect a single spectrum out of the DFT, but we get a spectrum plus its mirror image. The "second" spectrum starts at index

$k = N/2$. That means that we will automatically discard a set of $N/2$ points. We can find this peculiarity by substituting k by $N - 1$. Now, with the help of the identity:

$$e^{i2\pi k} = \left[e^{i2\pi}\right]^k = 1^k = 1 \tag{2.8}$$

we get the mirror symmetry as:

$$S\left(N - k\right) = S\left(-k\right) \tag{2.9}$$

where the folding wavenumber is:

$$\nu_f = \frac{n\Delta}{2} = \frac{1}{2\Delta x} \tag{2.10}$$

In fact, we can also extract that the equation 2.6 is valid for all k integers. If we replace k by $k + mN$ we get (equation 2.11 that the mirror symmetry is periodical and endless. We call the replication of the original spectrum an *alias*. Figure 2.3 shows us this behaviour.

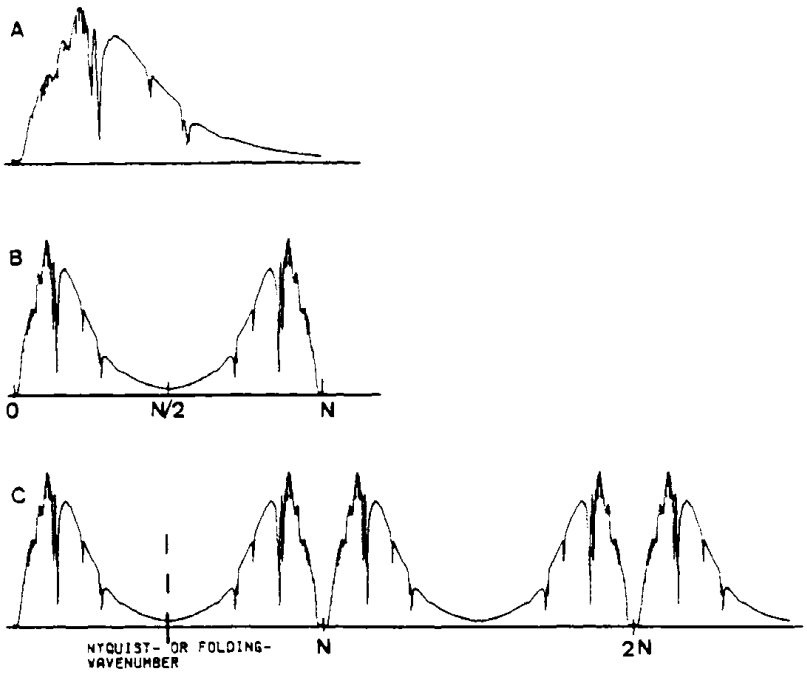

Figure 2.3: Effects of sampling. A) Expected shape of the spectrum. B) DFT yields to the spectrum and its mirror image. C) Aliasing: endless replication of B). Figure from [4]

$$S\left(k + mN\right) = S\left(k\right) \tag{2.11}$$

Problems from aliasing arise when the mirror spectrum overlaps with the desired spectrum. The problem will disappear if the spectrum is zero above a maximum wavenumber ν_max that has to be smaller than ν_f (equation 2.10). For a given wavenumber range, the FT-IR software will choose the maximum sample spacing in order to avoid overlapping.

Position Δx of the FT-IT are derived from zero crossings of a He-Ne laser wave with a wavelength $\lambda = 1/15800cm$. Zero crossings happen at $\lambda/2$ so Δx_{min} is $1/31600cm$. From equation 2.10 we get a folding wavenumber of $15800cm^{-1}$. It means that the maximum bandwidth we will be able to measure without overlapping will have a width of $15800cm^{-1}$. This will not be a problem for us as we will be measuring far more small bandwidths (from $370cm^{-1}$ to $5000cm^{-1}$).

As an ideal interferogram should be infinite, we can express a truncated interferogram at optical path difference $x = L$ by multiplying an infinite interferogram $Iin\,(x)$ by a function $B\,(x)$ that is zero for $x > L$. We have to do this because having $Iin\,(x)$ would mean an infinite range of movement of the mirror in the Michelson interferometer.

$$IL\,(x) = Ii\,(x)\,B\,(x) \tag{2.12}$$

If we define $Si\,(\nu)$ and $b\,(\nu)$ as the Fourier Transforms of $Ii\,(x)$ and $B\,(x)$ respectively and $SL\,(\nu)$ as the FT of IL and then apply equation 2.4, we get that the truncated spectrum is the convolution of the infinite optical path spectrum with the Fourier transformed boxcar.

$$SL\,(\nu) = Si\,(\nu) * b\,(\nu) \tag{2.13}$$

Intuitively one would take $B(x)$ to be a boxcar function. It can easily be found, using the definition or a Fourier Transform table, that:

$$b\,(\nu) = 2L\ \mathrm{sinc}\,(2\nu L) \tag{2.14}$$

In Figure 2.4 we can see that the instrument function $b\,(\nu)$ has a maximum centered at $\nu = 0$ but other side peaks. This lobes cause leakage of the spectral intensity. This is a problem

because these side lobes are an artifact created by the sudden truncation of the interferogram at $x = L$. So we want to reduce the peaks amplitude. This practice is called apodization.

In order to do that, we have to cut the interferogram more softly. In Figure 2.4 we can also see other examples of cutoff functions defined in Table 2.1. We see that apodization functions reduce the size of the side lobes compared to the boxcar function. But this improvement comes with a negative effect. Width at Half Height (WHH) increases with respect to the boxcar instrument function in apodization functions. This is a not desired behaviour since this width defines the best resolution achievable (if two spectral lines are to appear resolved from one another, they must be separated by at least the distance of their WHH, otherwise no dip will occur between them). Some information of other apodization functions can be also found in table 2.1.

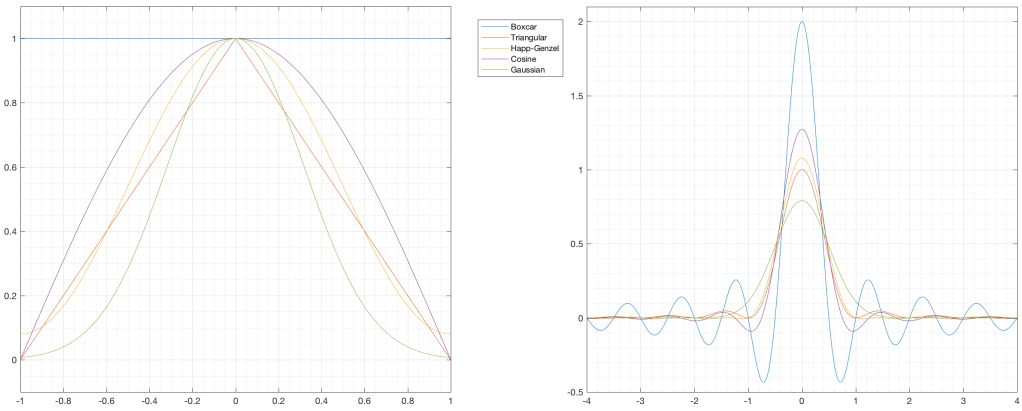

Figure 2.4: Some commonly used apodization functions and their instrument function. L=1 was used and instrument functions where normalised

Apodization Function ($\lvert x\rvert \leq L$)	Fourier Transform Image	FWHM	Resolution
Boxcar 1	$2L\,\mathrm{sinc}\,2\nu L$	$0.6/L$	$0.68/L$
Triangular $1-\frac{\lvert x\rvert}{L}$	$L\,\mathrm{sinc}^2\,\nu L$	$0.88/L$	$0.88/L$
Happ-Genzel $0.54+0.46\cos\left(\frac{\pi x}{L}\right)$	$\left(\frac{0.54}{\pi\nu}+\frac{0.464\pi\nu L^2}{\pi^2-(2\pi\nu L)^2}\right)\sin 2\pi\nu L$	$0.91/L$	$0.89/L$
Cosine $\cos\left(\frac{\pi x}{2L}\right)$	$\frac{\pi L}{(\pi/2)^2-(2\pi\nu L)^2}\cos 2\pi\nu L$	$0.82/L$	$0.85/L$
Gaussian $\exp-\left(\frac{2.23x}{L}\right)^2$	$\frac{L\sqrt{\pi}}{2.24}\exp\left(-\left(\frac{\pi\nu L}{2.24}\right)^2\right)$	$1.17/L$	$1.16/L$

Table 2.1: Some Apodization Functions with their FT, FWHM and resolution

We find another problem dealing with the measured interferogram. We would expect a real spectrum $S(\nu)$, but generally we get a complex spectrum $C(\nu)$. This is due to the asymmetry of the interferogram with respect to $x = 0$. This is originated by three different sources:

- We decided to get a single-sided interferogram. Only one side is recorded completely and only few hundred points are harvested from the other. Sometimes we decide to get a single-sided interferogram in order to reduce time spend measuring.
- When sampling, no position coincides exactly with the real zero path difference.
- The interferogram is asymmetric. This may be a consequence of wavenumber-dependent phase delays of the optics, the detector or the electronic filters.

So we want to extract the real spectrum. We can express the complex spectrum $C(\nu)$ as:

$$C(\nu) = R(\nu) + iI(\nu) \tag{2.15}$$

were $R(\nu)$ and $I(\nu)$ are real functions. Alternatively, we can also represent it as:

$$C(\nu) = S(\nu)\, e^{i\varphi(\nu)} \tag{2.16}$$

were $S(\nu)$ is the amplitude spectrum and $\varphi(\nu)$ is the phase. So we want to get the desired spectrum $S(\nu)$ from the actual output of the Fourier Transform $C(\nu)$. The first option would be:

$$S(\nu) = \sqrt{C(\nu)\, C^*(\nu)} = \sqrt{R^2(\nu) + I^2(\nu)} \tag{2.17}$$

This method would be correct for data without noise, but when we have noisy data, noise contribution is always positive if we use this method. In order to avoid that, we can take another expression. This method is called Merz method. From equation 2.16 we get that:

$$S(\nu) = \Re\Big\{C(\nu)\, e^{-i\varphi(\nu)}\Big\} \tag{2.18}$$

were the phase can be calculated as:

$$\varphi(\nu) = \arctan \frac{I(\nu)}{R(\nu)} \tag{2.19}$$

After all this data treatment, we can obtain the spectrum $S(\nu)$. This raw spectrum is not convenient for us to work with. We will rarely extract some useful information from it. This is due to the response of the machine that is frequency dependent, dimensionless and measures the emission from the sample and other external radiations such as the ambient radiation reflected by the sample or self emitted radiation from the FT-IR spectrometer. Water and CO_2 ambient molecules absorption alter pretty much the spectrum.

We will have to calibrate the measure in order to make these contributions disappear to raw spectrum. Each undesired radiation source will contribute with a different phase depending on the moment they get into the interferometer. This would be an extra problem, but using the data treatment commented on above we can solve this problem. Now, taking into account all the radiation sources, we can write the raw complex spectrum as [5]

$$\mathbf{S}(\lambda, T) = \mathbf{r}(\lambda) \left[e(\lambda) L_{BB}(\lambda, T) + r(\lambda) L_{amb}(\lambda) + \mathbf{L_0}(\lambda) \right] \tag{2.20}$$

where T is the sample temperature; $\mathbf{r}(\lambda)$ is the complex instrument responce function; $e(\lambda)$ is the sample emissivity and $L_B B(\lambda, T)$ is the Black Body radiance (with the definition of emissivity we know that $e(\lambda) L_B B(\lambda, T)$ is the sample radiance; $r(\lambda) L_{amb}(\lambda)$ is the radiance reflected by the sample; $r(\lambda)$ the reflectance of the sample; $L_{amb}(\lambda)$ the ambient radiance; and $\mathbf{L_0}(\lambda)$ the complex background radiance. We consider the radiance reflected by the sample and the emitted one to be real. In order to calibrate, we must determine the instrument response function $\mathbf{r}(\lambda)$ and the background radiance $\mathbf{L_0}(\lambda)$. We can determine them by measuring the radiation of a Black Body S_{BB} at two different temperatures T_L and T_H. Arranging equation 2.20 we get:

$$\mathbf{r}(\lambda) = \frac{\mathbf{S}_{BB}(\lambda, T_H) - \mathbf{S}_{BB}(\lambda, T_L)}{\mathbf{L}_{BB}(\lambda, T_H) - \mathbf{L}_{BB}(\lambda, T_L)} \tag{2.21}$$

$$\mathbf{L_0}(\lambda) = \frac{\mathbf{S}_{BB}(\lambda, T_L)}{\mathbf{r}(\lambda)} - L_{BB}(\lambda, T_L) \tag{2.22}$$

With the instrument response function and the background radiance we can rewrite equation 2.20 as:

$$e(\lambda) L_{BB}(\lambda, T) + r(\lambda) L_{amb}(\lambda) = \Re\left\{ \frac{\mathbf{S}(\lambda, T)}{\mathbf{r}(\lambda)} - \mathbf{L_0}(\lambda) \right\} \tag{2.23}$$

We take the real part in order to prevent noise from entering in the imaginary part. We still do not have the emissivity. To get it we will assume that the ambient radiance is the radiance of a Black Body at room temperature ($L_{amb} = L_{BB}(T_{amb})$, and that transmission of the sample is zero, $r(\lambda) = 1 - e(\lambda)$. The final equation for emissivity is:

$$e(\lambda) = \Re\left\{ \frac{\frac{\mathbf{S}(\lambda,T)}{\mathbf{r}(\lambda)} - \mathbf{L_0}(\lambda) - L_{BB}(\lambda, T_{amb})}{L_{BB}(\lambda, T) - L_{BB}(\lambda, T_{amb})} \right\} \tag{2.24}$$

2.2 Lock-In Amplifier

The thermal emission of a microsphere is a very small signal and since it will be buried in noise we will use a Lock-in amplifier. These amplifiers are used to detect AC signals; they use a technique known as Phase-Sensitive Detection (PSD) in order to find the signal at a reference frequency rejecting all other frequencies. This way, only the desired signal is detected. We will explain some details on this technique.

Let us suppose that the radiation we want to measure is oscillating at a fixed frequency. The Lock-In takes a reference signal oscillating at ω_r. It can generate it by itself or get it through a port. Let us assume that sample signal $V_s(t)$ and reference signal $V_r(t)$ are sinusoidal waves.

$$V_s(t) = V_{sig} \sin(\omega_s t + \theta_s) \tag{2.25}$$

being V_{sig} the signal amplitude.

$$V_r(t) = V_r \sin(\omega_r t + \theta_r) \tag{2.26}$$

The total signal entering the Lock-In amplifier can be expressed as:

$$V_{in}(t) = V_{sig} \sin(\omega_s t + \theta_s) + V_{noise}(t) \tag{2.27}$$

The Lock-In amplifies the signal and then multiplies it by the Lock-In reference signal. So the output of the Phase Sensitive Detection is [1]:

$$V_{PSD} = V_{sig} \sin(\omega_s t + \theta_s) V_r \sin(\omega_r t + \theta_r) + V_r \sin(\omega_r t + \theta_r) V_{noise}(t) \tag{2.28}$$

using basic trigonometric identities we get to:

$$V_{PSD} = \frac{V_r V_S}{2} \left[\cos\left((\omega_s - \omega_r) t + \theta_s - \theta_r\right) - \cos\left((\omega_s + \omega_r) t + \theta_s + \theta_r\right)\right] + V_r(t) V_{noise}(t) \tag{2.29}$$

Now, if both frequencies ω_s and ω_r are the same, this will lead to a DC component, an AC component at $2\omega_r$ and other AC components at unknown frequencies. After mixing both signals, Lock-In amplifier separates the DC component by the means of an adjustable low pass filter. The filtered output will be

$$V_{PSD} = \frac{V_r V_S}{2} \cos\theta \tag{2.30}$$

where $\theta = \theta_s - \theta_r$ is the phase difference between signal and the Lock-In reference oscillator. Some Lock-In amplifiers have a second PSD in order to eliminate this phase dependence. This new PSD multiplies the signal by the same wave as the first but shifted 90, so the resulting DC component for this PSD will be:

$$V_{PSD2} = \frac{V_r V_S}{2} \sin\theta \tag{2.31}$$

If we consider $V_r = 2$, the *in-phase* component $X = V_s \cos\theta$ and the *quadrature* component $Y = V_s \sin\theta$ we can remove phase dependence by computing the magnitude of the signal vector:

$$R = \sqrt{X^2 + y^2} = V_s \tag{2.32}$$

The low pass filter has two characteristics, bandwidth and filter order. The filter is a typical RC type filter. The filter bandwidth or $-3dB$ point is the cutoff frequency where the signal

power is divided by halfor is attenuated by $3dB$. This frequency is inversely proportional to the time constant τ.

$$f_{-3dB} = \frac{1}{2\pi\tau} \tag{2.33}$$

On the one hand, choosing a wide bandwidth will lead to fast measurements but will introduce systematic measurement errors as the ω component might be leaking to the output signal. A larger bandwidth means more noise and so a lower signal to noise ratio. On the other hand, a narrow bandwidth will reduce noise and increase signal to noise ratio but it will also increment time spend for the measurement. We have to choose wisely the time constant.

We can also adjust the order of the filter. A higher order leads to a more ideal rectangular filter transfer function that blocks frequencies outside the filter bandwidth more efficiently, but takes more time to settle to the final value. Wait time is the time required to get to 99% of the final value. Another interesting value is the equivalent noise bandwidth (ENBW). It is defined as the bandwidth of a brickwall filter which produces same integrated noise power as that of an actual filter. In table 2.2 some waiting times and ENBW are shown.

The sensitivity of the lock-in is the rms amplitude of an input sine (at the reference frequency) which results in a full scale DC output. For different measurements we will change this sensitivity. We will have to store the values for each measurement in order to make a correct calibration and to obtain different coefficients such as transmission coefficient or emissivity. The output of the lock-in is:

$$Output = (signal/sensitivity - offset)10V \tag{2.34}$$

Last relevant consideration on the Lock-In is the dynamic reserve that quantifies the capability of the Lock-In to reject unwanted signal component still providing accurate results. For example, with a dynamic reserve of $60db$, a $1\mu V$ signal with a specified accuracy of 1% nearby disturbance from up to $1mV$.

When combining Lock-in techniques with FT-IR spectroscopy, as our case, waiting time becomes a very relevant parameter to take care off. This is because, when using step scan mode, we have to wait after each step of the mirror. The sum of all waiting times can be very high

making measurements really slow. For example, if we want a resolution of $8cm^{-1}$ in a single-sided interferogram the mirror will have to take 4442 steps, and if we take a not very large time constant of $30ms$ we will have to wait $23min$ just for a single interferogram. Normally several interferograms are averaged in order to get a better spectrum.

Slope	ENBW	Wait Time
$6dB/oct$	$1/4\tau$	5τ
$12dB/oct$	$1/8\tau$	7τ
$18dB/oct$	$1/32\tau$	9τ
$24dB/oct$	$1/64\tau$	10τ

Table 2.2: Waiting times and ENBW for different filters from [1]

2.3 Experimental Set-Up

If we want to measure the thermal emission of a single micro we will need to heat it with a self-made accessory that must be placed outside the FT-IR spectrometer. Moreover, if we want to compare this radiation with respect to the radiation emitted by a black body, we must implement a set up for it. As already mentioned, the original plan has not been fully completed. Only the design and general considerations of optical set-up were carried out. In order to test the set-up we did a small modification of the final one to measure transmittance of a sample. This part of the total experimental set-up is fundamental to then add the thermal one. In this section, we will present a description of the set-up and all the changes made.

2.3.1 Optical Set-Up

A first transmittance set-up sketch is shown in Figure 2.5. The FT-IR spectrometer used has several input beam ports. We used the rear one (see Figure 2.6). The radiation we want to measure enters the spectrometer through a KBr window and then is collimated and directed to the interferometer by the mirror M_1. With the FT-IRs software we can easily configure the machine to use this port as the IR source. As we want to combine FT-IR spectrometer with the

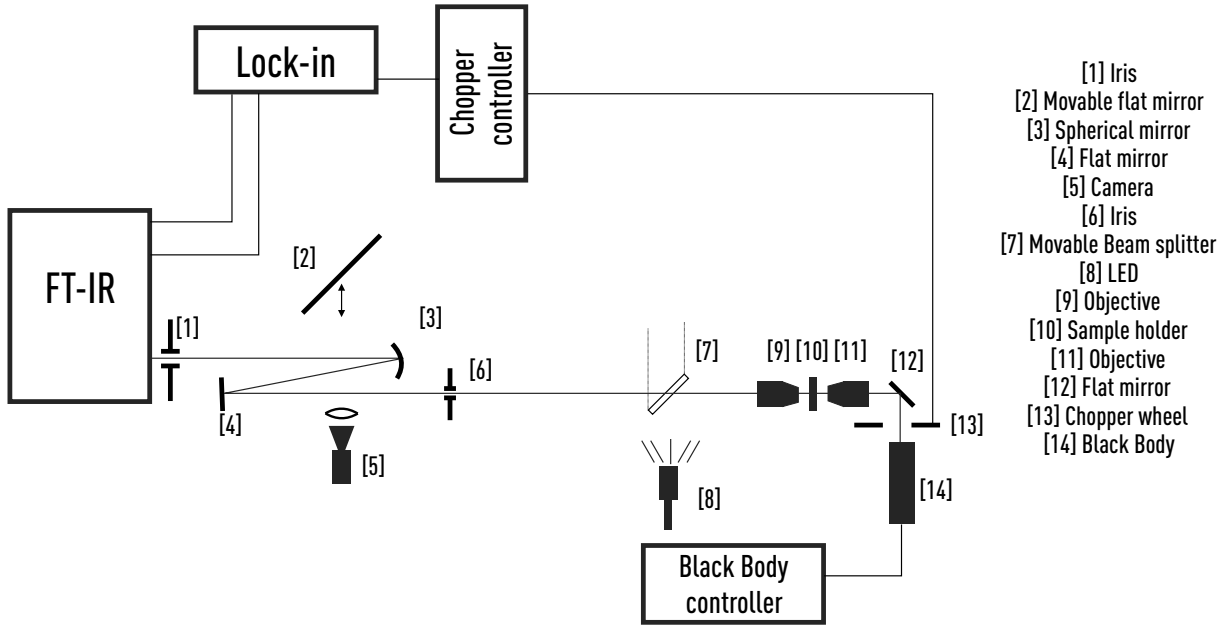

Figure 2.5: First transmittance set-up

Lock-In amplifier, we must configure the output of the detector via the AC out port to the input of the Lock-In and then bring back to spectrometer the final value via the DC in port. As we saw, we must extract the R value from the Lock-In. Again, this is easy to configure selecting the detector option to DC_IN. For the Lock-In to perform the Phase-sensitive detection it needs a signal at the reference frequency. This signal is provided by the chopper controller that also controls the modulation of the emitted radiation of the Black-body. An optical chopper interrupts periodically a light beam. It has a wheel with slot blades that cut the beam at a desired frequency. Different slot "designs" allow different frequencies. Figure 2.7 exemplifies the operation of this device.

The output signal is a square signal. In order to understand the demodulation processes at the Lock-In amplifier, we must use the Fourier theorem. It states that any periodic function can be expressed as an infinite sum of linearly independent sin and cos terms. The first term has the fundamental frequency that corresponds to the frequency of the square signal. Other higher frequencies correspond to harmonics, which will be removed by means of the low pass

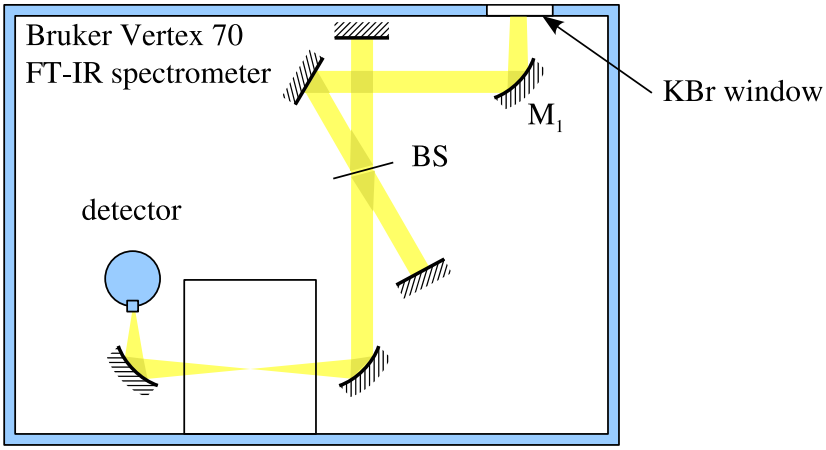

Figure 2.6: Michelson Interferometer and rear beam port in FT-IR in the Bruker Vertex 70 spectometer. From [5]

filter. The black body is placed at the largest optical path. By the help of a controller, we

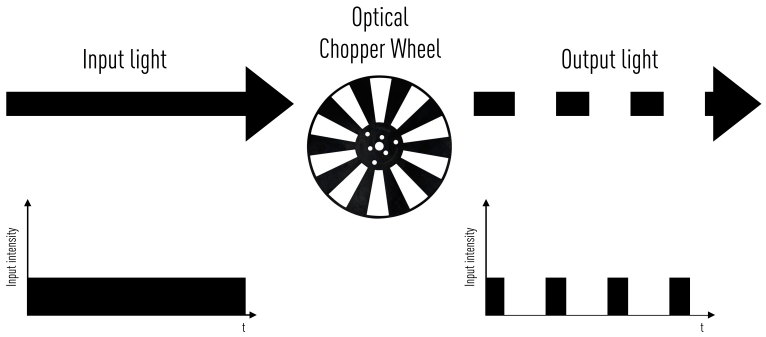

Figure 2.7: Chopper operation

can make this IR source emit as a Black Body at a selected temperature. It is an Infrared System Corporations IR-519 with an emittance greater than 0.99. We will use this radiation to calculate the transmission of different samples but also to calibrate the measures. The chopper wheel is placed just after the black body. At first, it was placed between the second objective and the iris due to space, but it chopped too much undesired light that also "survived" the PSD - we sent the radiation into the medium and then chopped it but it is better to send the chopped beam to the medium -.

Now, with the help of a flat mirror we bring the beam to the first objective. The black body was not placed with the beam exit directed towards the objective to try to minimise unwanted radiation entering the spectrometer. We use this objective to focus the radiation on the sample.

The sample is placed in a sample holder we had to design. This holder has a small hole to let radiation pass through the sample. This accessory is attached to a manual XYZ stage to adjust its position and bring the sample to the focal point of both objectives (See Figure 2.8). After passing thorough the sample holder, the light beam gets focused again at $160mm$ from the second. In this first set-up we did not place the iris at this distance. We did not place it at the mentioned distance in order to get a bigger magnification. The function of this iris is to "select" the area we want to measure - ideally, when measuring the thermal emission of the microspheres, we should close the iris andselect just the spheres emission-.

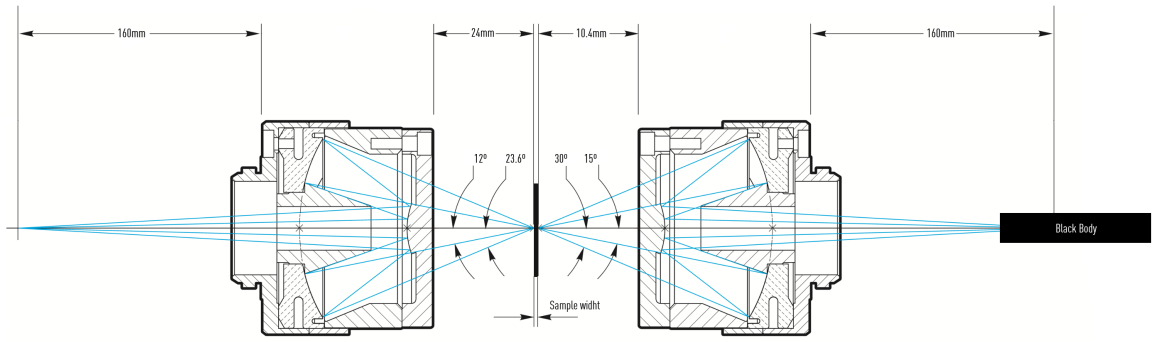

Figure 2.8: Ray diagram of the objectives

I order to adjust the area we are measuring, we use a CMOS camera with a lens of focal length $f = 100mm$ as shown in Figure 2.5. When we want to see the sample, we must bring the beam splitter to interact with the ray (note that the position of the beam splitter when measuring is away from the optical path). We illuminate the sample with a LED. The visible light travels to the beam splitter splitting light into two new beams. One is transmitted and not useful and the other gets reflected and focused by the objective. Now the sample reflects this light and gets focused at the camera by the lens already mentioned. The moving mirror is used so that the camera is not placed in the optical path of the radiation when measuring.

After the iris, two gold mirrors are placed in order to focus the radiation in the second iris next to the spectrometer so that we can remove external radiation. Figure 2.10 shows a schema of the equivalent optical set-up. This iris is set at the point that the internal optics of the FT-IR focuses the radiation at the detector. The actual set-up can be seen in Figures 2.11 and 2.12.

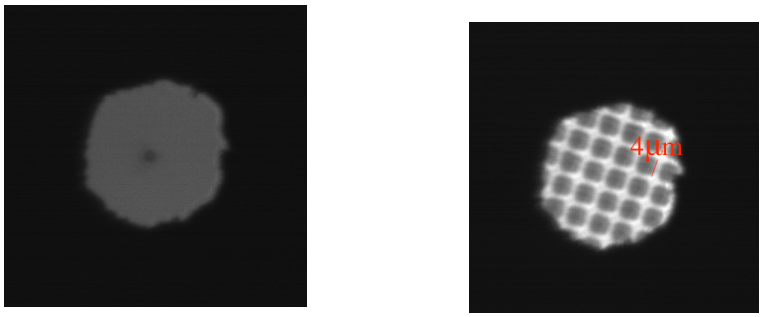

(a) (b)

Figure 2.9: a) Image of the "ruler" used to know the measuring area and b) Image of a Silicon microsphere from our microscope

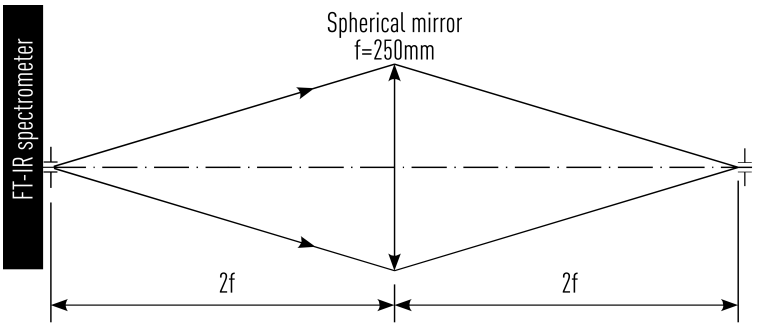

Figure 2.10: Equivalent optical system for the optical path between both irises

The process of aligning the set-up was first done with a light fiber, setting it at the sample compartment of the spectrometer. This beam focused at the second iris and then should focus again at the Black body and we went step by step aligning each component. After that, due to the low intensity of this light, we decided to use a laser to make the precise alignment.

A first possible modification of the set-up is not very different than the first one. The only change is the first objective and flat mirror next to the Black Body for a spherical one as we can see in Figure 2.13. This set-up would compensate the fact that both objectives are not the same and have different collection angles.

The second modification of the set-up is directly putting the Black Body (and the chopper) behind the sample, without any mirror or objective before the Black Body radiation impinges the sample. Also placing the objective at $160mm$ from the iris to take profit of all the solid angle of the objective and getting a stronger signal would be a reasonable idea, though it would mean a lower magnification that would entail a bigger area of measurement if the iris was not

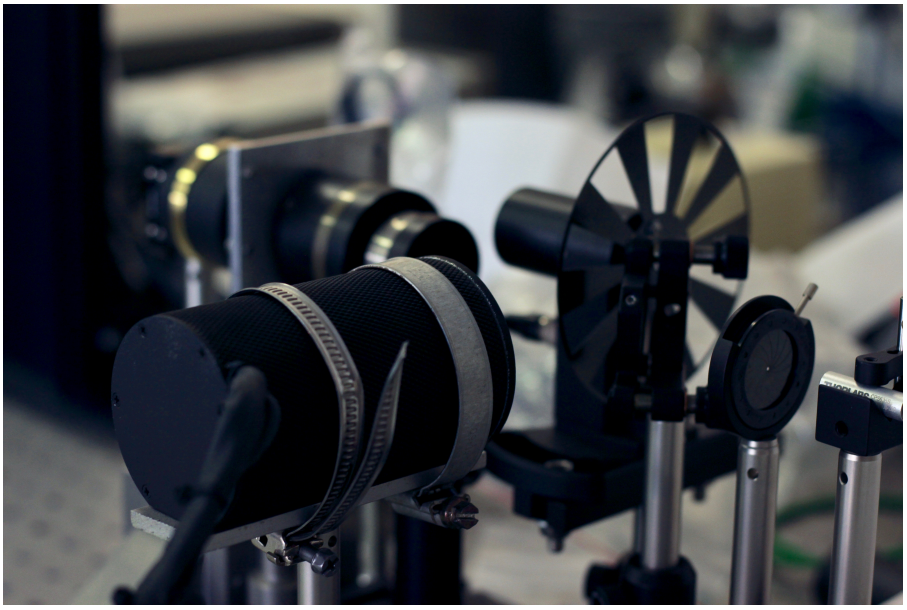

Figure 2.11: Detail of the first set-up. We can see the Black Body, the laser used to align the setting, the chopper wheel, both objectives and the sample holder.

changed for a pinhole.

2.3.2 Thermal Set-Up

The study of the thermal emission of Silicon microspheres would need a last change on the set-up. The sample with the microspheres would be placed at the same spot where the sample holder is. The chopper would have to be placed between the sample and the objective since our new IR source will be the microspheres themselves. So the Black Body will no longer be our source, but it will still have its spot in the set-up in order to calibrate the measurements. As the goal is to measure the emission of a single sphere and that is not possible for us, changing the iris for a pinhole smaller that the iris is a reasonable idea.

The biggest challenge concerns the actual heating of the microsphere due to its small size. The accessory must be able to determine the real temperature of the sphere. Also problems emerge from the thermal radiation of the substrate where the microspheres are placed. This radiation will be significantly large and the signal from it will be also getting to the Lock-In oscillating at the reference frequency.

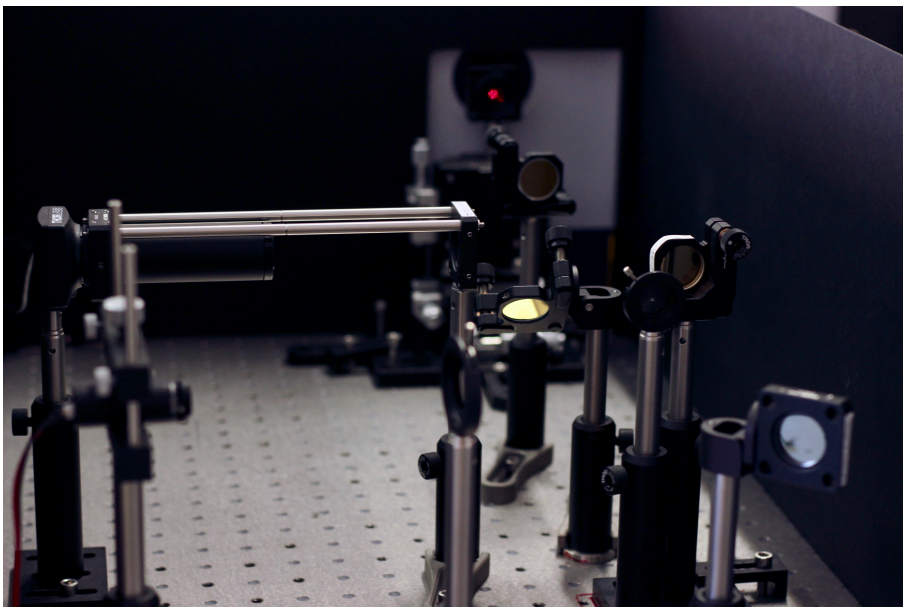

Figure 2.12: Detail of the first set-up. We can see the beam splitter, the LED used to illuminate the sample, both irises, the camera and the rear input beam port of the FT-IR spectrometer.

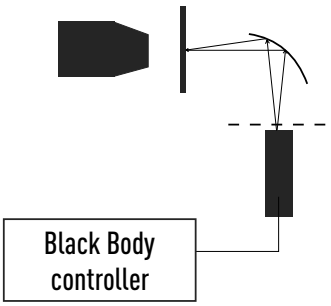

Figure 2.13: First modification of the set-up

A possible idea to reduce this unwanted thermal radiation, the microspheres could be attached to a substrate with low emissivity, maybe a metal. Another idea to avoid thermal radiation from the substrate could be the heating of the microsphere with the help of a laser. This would reduce substrate radiation since we would be heating directly the microsphere. The problem from this procedure is the precise determination of the temperature of the sphere. Knowing the temperature is very important in order to prove that the particles have an absorption higher than one. As we already said this would mean an emissivity higher than a Black Body at that temperature. In order to compare the radiations we need to configure the Black Body at the exact temperature, if not, we would see resonances in the thermal radiation spectrum of the microspheres but we could not acquire emissivity.

Another possible approach to the thermal measurement could be to separate the spectrum of the microsphere by means of a piezo stage in order to make oscillate the microsphere mechanically. The substrate with the particle would enter and exit the measuring area. With this solution no chopper would be necessary, as the signal that the detector gets would oscillate as a sinusoidal function with an offset - this offset would be the value of the detectors output when no microsphere is present in the measuring area but only the substrate-.

Moreover, a more complex system could be tested. This set-up would consist of two pinholes that would select two different measuring areas of the sample. One with a microsphere and the other one without it. We should chop the signal in order to just detect the contribution of one pinhole at a time. Like the solution with the piezo stage, the oscillating component of the signal will be the contribution of the microsphere.

Chapter 3

Results and Discussion

As commented on throughout the text, the main aim of the project has become the design -and the successive adjustments- of the optic set-up which, in the future, will let measure thermal radiation of the silicon microspheres mixing Step Scan FT-IR spectroscopy together with lock-in techniques.

Two of the main factors that have conditioned this research have been time and noise. Time has conditioned not only the duration of the project itself but also the duration of the measurements to test that we were approaching a valid set-up for the requirements of the experiment. In order to get an understandable result we need to make three measurements. We need the spectrum we want to know and also two extra spectra of the Black Body for calibrating the raw data we get.

The problem concerning noise is closely related to time. For some sources of noise, if we want to reduce it we need to get tens of spectra to average to zero this noise. This means making the measurement even more slow. However, there are some intrinsic source of noise from the lock-in and the spectrometer that we cannot eliminate.

In order to reduce measurement time, and as already commented on, data was not acquired for all possible negative displacement x, only for a few steps of the mirror and the complete positive x range. This should not be a problem as we saw that, ideally, the interferogram is

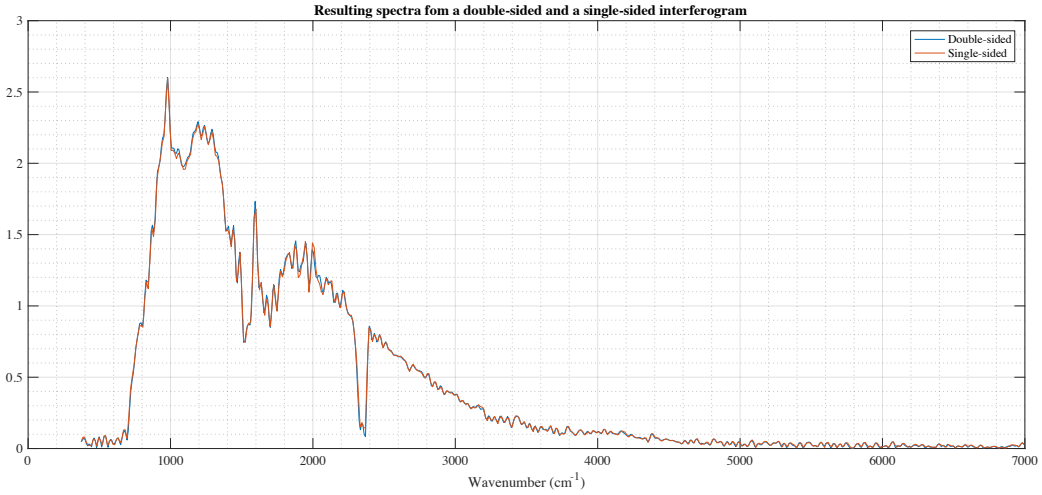

Figure 3.1: Resulting raw spectra of the emission of a Black Body at $700K$ for a double-sided and a single-sided interferogram of the same measurement

symmetric with respect to $x = 0$ but real ones were not symmetric.

In Figure 3.1 we can see that the spectra from the single-sided and double-sided interferograms differ a bit. Measuring time of the double-sided interferogram almost doubles the time of the single-sided one. The total measurement used to get this spectrum was one hour and twenty-six minutes. So we decided to go with single-sided interferograms. As a note, in this spectrum we can see approximately water vapour and CO_2 absorption bands between $1000cm^{-1}$ and $2000cm^{-1}$ and between $2310cm^{-1}$ and $2380cm^{-1}$ respectively.

Resolution of the measurement also affects dramatically the time of the measure since doubling the resolution doubles the number of points. This is a problem since we should set a quite high resolution in order to see peaks of absorption/emission of the microshperes.

In order to test the set-up, we measured the transmission coefficient of different elements already characterised. In order to calculate this coefficient we have to measure a Black Body radiation at a desired temperature with and without a sample in the sample holder. As always, two more Black Body radiations without sample must be measure to calibrate results.

When analysing the obtained data, we have to take into account the sensibility from the lock in to be able to compare spectra as we discussed. When doing this analysis we encountered some problems. As seen in Figure 3.2 and 3.3, the shape of the obtained transmission coefficient is

correct, but absolute value is not. The "real" transmission coefficient was measured in Rapid Scan in the FT-IR spectrometer with a measuring area of approximately $85mm^2$. When

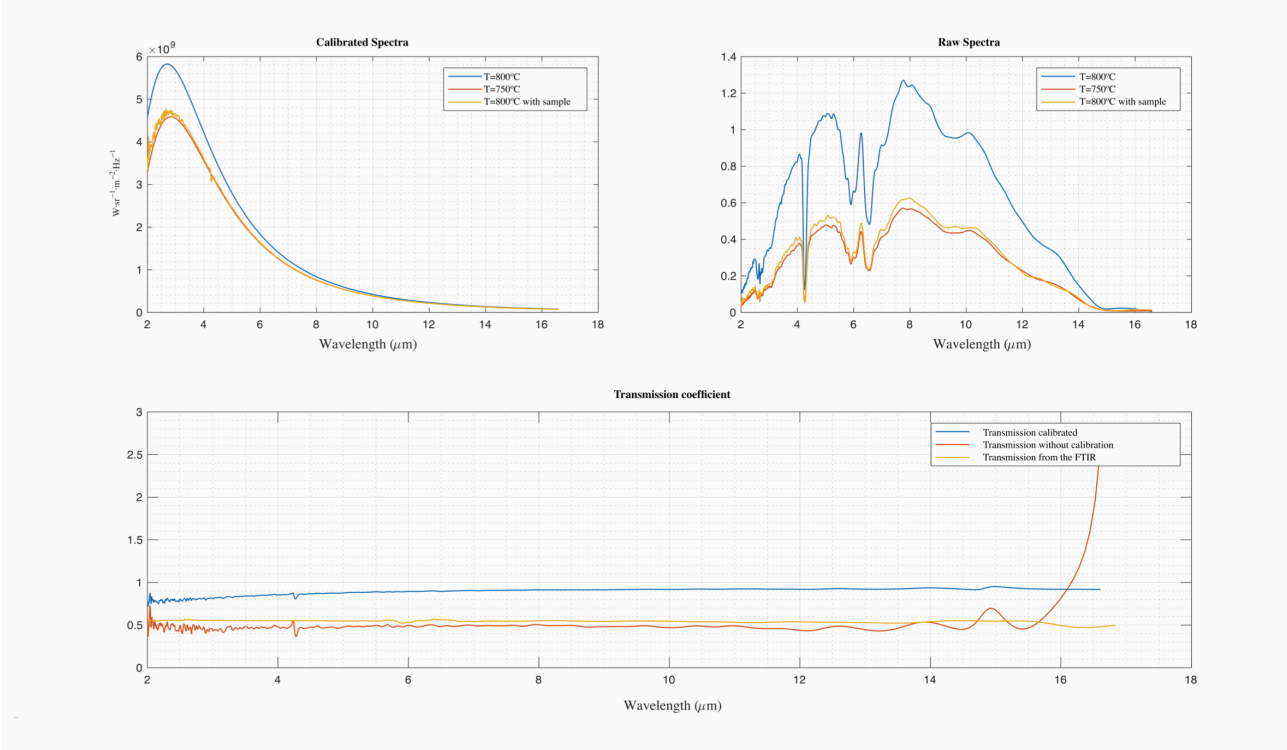

Figure 3.2: Calibrated spectra, raw spectra and transmission coefficient of a slice of Silicon

placing some samples in the optic path - for instance, the ones we wanted to characterise -, the lock-in received more signal than when the samples were not there and the signal that entered the lock-in was directly from the Black Body. When this happened, the lock-in got overloaded and we had to chance the lock-in sensitivity. This makes it impossible to get a reliable transmission coefficient, though the shape is correct. We were not able to find a correct explication for this behaviour, but we suspect it is an optical problem that further modifications of the set-up must eliminate.

With the last adjustment we made of the set-up and fine alienation we obtained the radiation of the Black Body at different temperatures (Figure 3.4). For this measure a time constant $\tau = 30\,ms$ was used. Data used to calibrate the measure correspond to the Black Body radiation at $850K$ and $650K$, that is why the measured spectra have a 0% relative error. Experimental

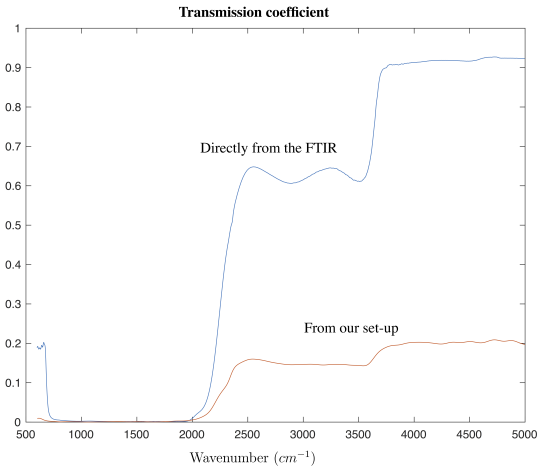

Figure 3.3: Transmission coefficient of a cover glass

data is plotted as dots and theoretical spectra are plotted as solid lines. The area measured was of the order of 300 μm^2. We know the approximate measured area by using the microscope of the set-up with a sample in the sample holder which has a pattern of known measures as seen in Figure 2.9 a).

In normal FT-IR spectroscopy, a typical measuring area of the order of $10mm^2$ is detected. This means that the signals detected with our set-up had 10^{-3} % of power than normally detected signals using normal FT-IR configuration. Though the relative error of the measure is quite low - 1% in most part of the spectra- we still should decrease this error.

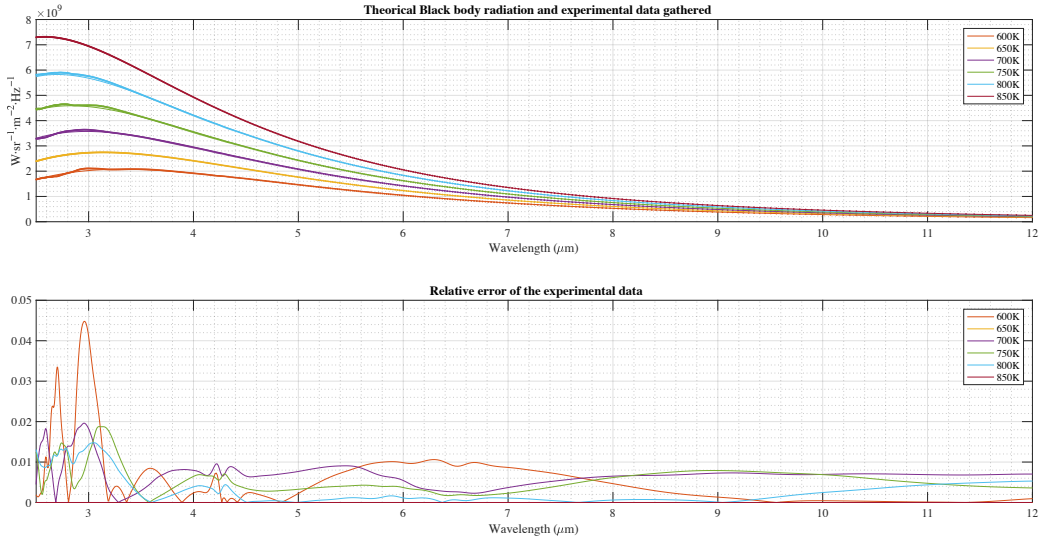

Figure 3.4: Black Body radiation measured at different temperatures

Chapter 4

Conclusion

Initial goals of the project were not accomplished. Since the thermal set-up for the measurement of the thermal radiation of a Silicon microsphere was not carried out. This objective was difficult to achieve. Though a great advance on the optical set-up for this measurement was reached.

Time has played a determinant role in this project. The realisation of the project was indeed conditioned to characteristic time of the measurements themselves - that were necessary to make small modifications in order to improve the implementation of the set-up- and unavailability of lab equipment for a relative long period.

Taking into account all the factors we did get some reasonably successful results as we were able to measure radiation with 0.001 of the power measured on normal mode in FT-IR spectrometers. All this was possible by combining Step-Scan FT-IR spectroscopy and lock-in techniques. Much more research ought to be carried out. Nevertheless, this project means a great start to be able to measure the thermal radiation of the Silicon microspheres.

Bibliography

[1] Stanford Reserch Systems. *MODEL SR830 DSP Lock-In Amplifier*. Sunnyvale, California.

[2] M. Garín et al. All-silicon spherical-mie-resonator photodiode with spectral response in the infrared region. *Nature Communications*, 5(3440), 2014.

[3] W. Spitzer et al. Infrared absorption in n-type silicon. *Physical Review*, 108(2), 1957.

[4] J.Gronholz and W. Herres. Understanding ft-ir data processing: Details of the spectrum calculation. *Instruments Computers*, 3(10), 1985.

[5] M. Garín. *Engineering the Thermal Emission of Macroporous Silicon*. PhD thesis, Universitat Politècnica de Catalunya, 2009.

[6] M. Tymczenko. *Photonic microcavities and photonic sponges based on silicon colloids*. PhD thesis, Universitat Politècnica de València, 2010.

[7] M. Garín et al. Light harvesting by a spherical silicon microcavity. *Journal of Applied Physics*, 119(033101), 2016.

[8] F. Messeguer et al. Silicon colloids: A new enabling nanomaterial. *Journal of Applied Physics*, 109(102424), 2011.

[9] D. Hernàndez. *Selective Thermal emitters based on photonic crystals*. PhD thesis, Universitat Politècnica de Catalunya, 2014.

[10] Q. Fu and W. Sun. Mie theory for light scattering by a spherical particle in an absorbing medium. *Applied Optics*, 40(9), 2001.

[11] S. Asano and G. Yamamoto. Light scattering by a spheroidal particle. *Applied Optics*, 14(1), 1975.

[12] W. Herres and J. Gronholz. Understanding ft-ir data processing: Data acquisition and fourier transformation. *Comp. Appl. Lab*, 4(216), 1984.

[13] T.J. Johnson. *Introduction to Step-scan FTIR*. Bruker, Billerica, Massachusetts.

[14] Eric Y. Jiang. Phase-, time-, and space-resolved step-scan ft-ir spectroscopy. *SPECTROSCOPY*, 1(17), 2002.

[15] R. Bracewell. *The Fourier Transform and Its Applications*. McGraw Hill, Stanford, California,.